Tetrahedral Pt 10 – Cluster with Unique Beta Aromaticity and Superatomic Feature in Mimicking Methane

Article *in* Journal of Physical Chemistry Letters · May 2021

DOI: 10.1021/acs.jpclett.1c01178

CITATION
1

READS
104

5 authors, including:

Jia Yuhan
Chinese Academy of Sciences
15 PUBLICATIONS **86** CITATIONS
SEE PROFILE

Hanyu Zhang
Chinese Academy of Sciences
26 PUBLICATIONS **228** CITATIONS
SEE PROFILE

Zhixun Luo
Chinese Academy of Sciences
158 PUBLICATIONS **1,888** CITATIONS
SEE PROFILE

THE JOURNAL OF PHYSICAL CHEMISTRY LETTERS
A JOURNAL OF THE AMERICAN CHEMICAL SOCIETY

pubs.acs.org/JPCL

Letter

Tetrahedral Pt_{10}^- Cluster with Unique Beta Aromaticity and Superatomic Feature in Mimicking Methane

Yuhan Jia,[†] Xinlei Yu,[†] Hanyu Zhang, Longjiu Cheng,* and Zhixun Luo*

Cite This: *J. Phys. Chem. Lett.* 2021, 12, 5115–5122

Read Online

ACCESS | Metrics & More | Article Recommendations | Supporting Information

ABSTRACT: Utilizing a customized metal cluster source in tandem with a flow tube reactor and a reflectron time-of-flight mass spectrometer, we have obtained well-resolved pure metal clusters Pt_n^- and observed their gas-phase reactions with a few small gas molecules. Interestingly, the remarkable inertness of Pt_{10}^- was repeatedly observed in different reactions. Meanwhile, we have determined the structure of Pt_{10}^- within a regular tetrahedron. Considering that Pt possesses $5d^96s^1$ electron configuration, the tetrahedral Pt_{10}^- exhibits unexpected stability at neither a magic number of valence electrons nor a shell closure of geometric structure. Comprehensive theoretical calculations unveil the stability of Pt_{10}^- is significantly associated with the all-metal aromaticity. In addition to the classical total aromaticity, which is mainly due to 6s electrons, there is unique beta-aromaticity ascribed to spin-polarized beta 5d electrons pertaining to singly occupied multicenter bonds. Further, we demonstrate the superatomic feature of such a transition metal cluster Pt_{10}^-, as $Pt_6@Pt_4^-$, in mimicking methane.

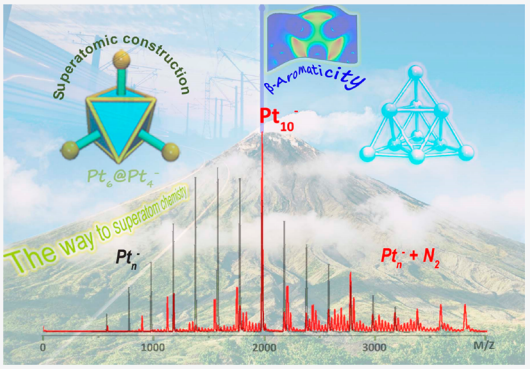

Single platinum atoms and Pt-related complexes have been widely applied as catalysts in fuel cells,[1] gas reforming,[2] automotive three-way conversion,[3,4] and various redox reactions,[5,6] as well as medical uses as anticarcinogen,[7] aural, or retinal implants. A majority of such studies have also revealed significant advantages of Pt-related catalysts and drugs at reduced sizes of nanoscale. However, the non-negligible relativistic effect of Pt, novel metal bonding nature and solvent effect in sol−gel preparation make it difficult to fully understand the precise mechanism simply by extension of knowledge based on single atoms or Pt-complexes. A key task to rationally design nanocatalysts and to understand the underlying mechanism has fallen on cluster science. Motivated on this, metal clusters have attracted enormous attention over the past decades, with an increased rate of specific surface area and low cost of such precious metal,[8−11] available for precise chemistry research of reaction mechanism, chemical stability and bonding nature, in joint with first-principles theoretical calculations.[12−14]

A pending issue is that the catalytic performance of metal clusters could be reduced in the atmosphere because of the adsorptive contamination or a failure to maintain the anticipated geometric and electronic structures. A basic understanding of the factors that determine the stability, property, and reactivity of atomic clusters is important for the establishment of fundamental principles and craft at reduced sizes.[15,16] Ongoing efforts have been paid to explore magic clusters with resistance to oxidation and contamination. A few magic metal clusters, such as Al_{13}^-, Ag_{17}^-, $Al_{11}Mg_3^-$, etc., have been found to survive rich-pressure oxygen etching reactions,[17−20] and are associated with closed electronic (and geometric) shells.[21] Meanwhile, some other metal clusters, such as Ag_{13}^-,[17] and Cu_{18}^-,[22] were also found to be inert in reacting with oxygen, shedding light on superatomic stability.[23−25] Among others, the previous studies found low activity of Pt_{10}^+ and Pt_{14}^+ in the reaction with CH_4 and N_2O at a low partial pressure of $\sim 10^{-3}$ mPa;[12,26] also for the anionic Pt_n^- clusters, local minimal points of rate constants were estimated for the Pt_6^-, Pt_{10}^-, and Pt_{14}^- clusters.[26] In comparison, Pt_8^- and neutral Pt_8 were found to be reactive with N_2O.[26,27] Among others, the spin dynamics of a ring-shaped Fe_{10} cluster compound has been studied by inelastic neutron scattering, showing novel magnetic anisotropy of such a ten-atom cluster.[28]

However, even if do not consider the atomlike behavior and identity of superatomic nanoclusters in conjunction with ligands,[23] there is a difficulty to estimate the valence electron counts for transition metal clusters (because of the complexity of d and f electrons) and to predict their cluster stability with magic numbers. In particular for heavy transition metals, the

Received: April 13, 2021
Accepted: May 19, 2021

https://doi.org/10.1021/acs.jpclett.1c01178
J. Phys. Chem. Lett. 2021, 12, 5115−5122

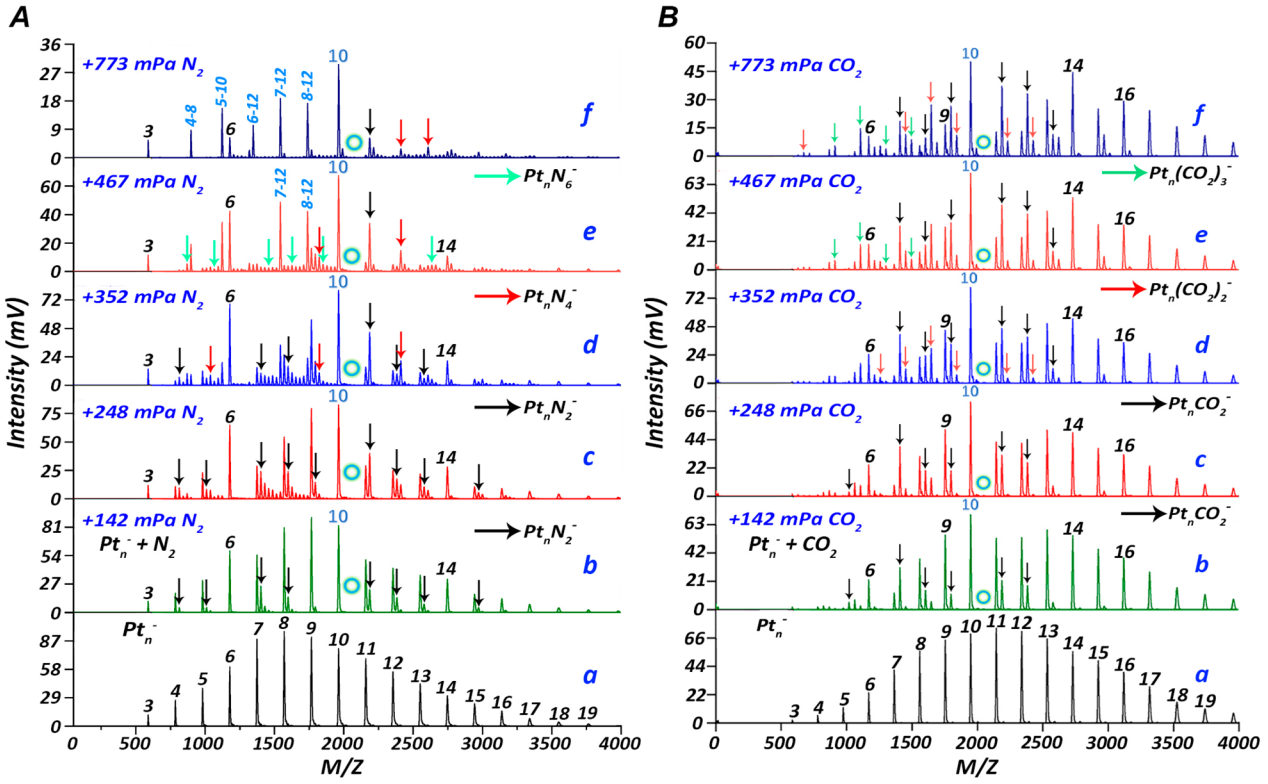

Figure 1. (A) Mass distributions of Pt_n^- clusters in the (a) absence and (b–f) presence of a different amount of N_2 gas with the partial pressure at 142, 248, 352, 467, 773 mPa, respectively. (B) Mass distributions of Pt_n^- clusters in the (a) absence and (b–f) presence of a different amount of CO_2 gas with the partial pressure at 142, 248, 352, 467, and 773 mPa, respectively. The pure Pt_n^- clusters are labeled as number *N*.

multicenter electron delocalization to form superatomic orbitals could be even more complex because of the orbital hybridization and mixed partition of contributions by both alpha and beta spin electrons.[29] Note that, the exploration of stable metal clusters with resistance to small molecule adsorption is important for anticorrosion in micro devices. In particular, noble metals, such as Pt atoms and cations, readily form coordination bonds with various ligands. Although a challenging task, it is important to prepare pure platinum metal clusters and fully study their size-dependent stability and reactivity under sufficient collision reactions.

Having this in mind, we have conducted a gas-phase reaction study to explore the stability of small Pt cluster anions. We prepared Pt_n^- (n = 3–19) clusters with a good mass resolution by a homemade laser vaporization (LaVa) cluster source,[30] and undertook a comprehensive study on the reactions of Pt_n^- with N_2, O_2, CO_2, and CH_3Br. Among them, oxygen readily reacts with Pt_n^- clusters to produce various oxides; CH_3Br reacts to produce hydrogen; and N_2 and CO_2 react to form $Pt_nN_{2m}^-$ and CO_2-addition products. What is interesting is that, among all the reactions, Pt_{10}^- finds prominent mass abundance and is inert to all these chemicals (except O_2 adsorption). Utilizing DFT calculations, we unveil the unique stability of Pt_{10}^- with a global minimum structure of tetrahedron and unique beta aromaticity.[31] Also, we provide a comparison regarding the aromaticity of $Pt_{10}^{\pm,0}$ versus Au_{10}^{2+}, as well as Pt_6^- versus Au_6; further, we demonstrate the origin of all-metal aromaticity on multicenter bondings and superatomic feature with Pt_{10}^- in mimicking methane.

We have managed to prepare ionic $Pt_n^{\pm}$ clusters (n = 3–19) via a customized LaVa metal cluster source and studied their reactions with a few common gas molecules. Figure 1A presents the mass spectra of the obtained Pt_n^- clusters in the absence and presence of different amounts of N_2 reactants. It is notable that most anionic Pt_n^- clusters readily react with N_2 and form $Pt_n(N_2)_m^-$ adducts, but $Pt_{3,6}^-$ and Pt_{10}^- are inert toward dinitrogen. In particular, Pt_{10}^- dominates the mass distribution in the presence of a large flow rate of N_2 (with a partial pressure up to 773 mPa) showing its distinction in surviving the reactions of rich-pressure gas collisions. Note that, the relative intensities of Pt clusters larger than Pt_{10} drops under higher pressures due to the likely collision-induced dissociation of larger Pt_n clusters, as well as the charge annihilation caused by the collisions with the inwall of the flow tube, along with likely etching-like reaction channel (e.g., $Pt_n^- + mN_2 \rightarrow Pt_{n-1}^- + Pt(N_2)_m$, for details see Table S4). Similar inertness of $Pt_{3,6,10,14}^-$ have also been observed in the reactions with CO_2 (Figure 1B), where the other sized Pt_n^- clusters react to form products of CO_2 addition, $Pt_n(CO_2)_m^-$. In addition, we have also studied the reactions of cationic Pt_n^+ clusters and found they prefer to attach N_2 molecules; also, Pt_{10}^+ is relatively inert (Figure S3), which is consistent with the previously reported reactions with CH_4.[12]

We have chosen a few other reactants, including O_2 and CH_3Br, to further probe the stability of Pt_n^- clusters. As results, the stability of Pt_n^- clusters is difficult to be screened out by O_2 etching (Figure S4). However, with a large flow rate of CH_3Br being introduced into the flow tube reactor, Pt_{10}^- emerges again as the dominant species observed in the mass spectra (for details see Figure S5). This is in sharp contrast to its neighboring counterpart clusters, such as Pt_{7-13}^-, which are reactive and form varied products involving molecule adsorption, dehydrogenation or oxygen reduction, respectively.

https://doi.org/10.1021/acs.jpclett.1c01178
J. Phys. Chem. Lett. 2021, 12, 5115–5122

The dominant channels for these tested reactions are summarized as

$$Pt_n^- + mN_2 \rightarrow Pt_n(N_2)_m^- \quad (1)$$

$$Pt_n^- + mO_2 \rightarrow Pt_n(O_2)_m^- \quad (2)$$

$$Pt_n^- + mCO_2 \rightarrow Pt_n(CO_2)_m^- \quad (3)$$

$$Pt_n^- + mCH_3Br \rightarrow Pt_n(CHBr)_m^- + mH_2 \quad (4)$$

In terms of the above four reaction channels, the first three reactions exhibit only an absorption behavior, which could be considered as the pseudo-first-order reaction. The rate constants k for Pt_n^- reacting with N_2 and CO_2 have been estimated and provided in Figure S2. As clearly indicated by the mass spectral distribution, the k values of Pt_6^- and Pt_{10}^- are significantly small pertaining to their reduced chemical activities. Besides, unlike other clusters of the main group metals or light transition metals, here the reactivity and stability of Pt_n^- clusters do not fully support the observation of odd−even oscillating behavior because of the varied spin multiplicity and electronic configuration. It is supposed that, to some extent, the jellium model based on the near-free electron gas theory could be not sufficient to explain their reactivity and stability. Also, the principles based on valent electron counts (e.g., 8, 18, or 40 electron stability) could not well predict the experimental results in gas-phase reactions.

A series of structures for Pt_n^-, Pt_n, and Pt_n^+ (n = 2−15) clusters with different spin multiplicities are obtained via global search (Figure S6−9). With a focus on the Pt_n^- clusters, Figure 2a and b display the geometry of Pt_{10}^- and electronic properties of Pt_n^- (n = 2−14) clusters, where the HOMO−LUMO gaps, incremental binding energies (IBE), and second-order binding energy (Δ_2E) of the global minimum Pt_n^- clusters display local maximum at n = 6 and n = 10. Also, we have performed Born−Oppenheimer molecular dynamics (BOMD) simulations to further test the dynamic stability of Pt_{10}^-, as shown in Figure 2c (more details in Figure S22). As results, the pseudo-T_d structure of Pt_{10}^- is dynamically stable at 300, 600, 900 and even 1200 K during MD simulations up to 5 ps (i.e., 5 thousand steps), showing small values of the root−mean−square−deviation (RMSD) and the maximum bond length deviation (MAXD) on average. In addition, the N_2-binding energies on Pt_n^- (n = 2−11) clusters find local minima values at n = 3, 6, and 10 (Figure 2d). The prominent HOMO−LUMO gaps, IBE, Δ_2E, and the smaller N_2-binding energy denote the stability of the three clusters (Pt_3^-, Pt_6^-, and Pt_{10}^-), which is well consistent with the experimental observation.

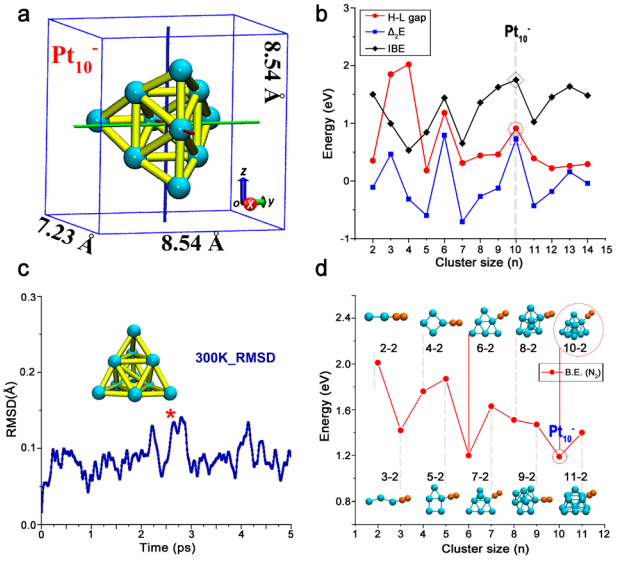

Figure 2. (a) VDW radius of Pt_{10}^- calculated by Multiwfn program, in which VDW surface is defined by the three sides of the cube. (b) Calculated HOMO−LUMO gaps of α orbitals (red), Δ_2E (blue), and incremental binding energies (black) of Pt_n^- (n = 2−14) clusters. (c) Born−Oppenheimer molecular dynamics (BOMD) simulations of Pt_{10}^- at 300 K (see Figure S22 for results at 600, 900, and 1200 K), using the CP2K software package with the time step of 5 fs at the PBE/DZVP level, starting from the equilibrium GM geometry with random velocities assigned to the atoms, with the average root-mean-square-deviation (RMSD) values of bond lengths indicated in Å. (d) Calculated N_2-binding energies onto the Pt_n^- (n = 2−11) clusters. The lines are drawn to guide the eye.

Considering the electron configuration of Pt ($5d^96s^1$) and the high spin multiplicities of the platinum clusters, we have studied α and β electrons separately to unveil the chemical bonding. First, $^4Pt_3^-$ cluster has three unpaired single spin electrons, that is, three more α electrons than β electrons. As shown in Figure 3a, the d orbitals of the linear $^4Pt_3^-$ cluster locate on the Pt atoms at both ends and are filled with both α and β electrons (d^{5+5}); while the orbitals correlative to the central Pt atom are occupied with five α electrons and two β electrons (d^{5+2}). The α and β electrons pair up in the outermost s orbitals, forming two 3c−2e bonds (for details see Figure S26). In comparison, the neutral $^3Pt_3$ cluster has a triangular shape, where the d electrons of each Pt atom occupy five α orbitals and four β orbitals first (d^{5+4}), and the rest d electrons of β orbitals delocalize on three Pt atoms, forming a 3c-1e bond; meanwhile, the α and β electrons pair up in the outermost s orbitals and form a 3c-2e multicenter bond (Figure S27).

Similarly, the d orbitals of both neutral $^7Pt_6$ cluster and anionic $^6Pt_6^-$ located on the outside three Pt atoms are filled with α and β electrons (d^{5+5}), while the three Pt atoms in the middle are occupied with five α electrons and three β electrons (six electrons less). For $^7Pt_6$ (Figure S28), the β electrons are six less than α electrons, while for $^6Pt_6^-$, the beta d-electrons on the central Pt atoms form a 3c−1e bond, which means that β electrons are five less than α electrons. Such a single-occupied multicenter bond of β 5d electrons illustrates a unique beta-aromaticity, which was not noted in previous studies to the best of our knowledge. In addition, the α and β electrons also pair up in the outermost s orbitals on the whole molecule, forming three 6c−2e bonds (Figure S29). On this basis, the number of both unpaired single-spin β electron and the three paired electrons complies with the general Hückel ($4n$+2) rule.

As shown in Figure 4, we have also calculated the nucleus-independent chemical shift (NICS),[32,33] which is used as a criterion to evaluate the molecular aromaticity. For the planar Pt_6^- and tetrahedral Pt_{10}^- clusters, the NICS diagrams reveal a considerable negative value. It is indicative of strong aromaticities of the Pt_6^- and Pt_{10}^- clusters pertaining to all-metal inorganic aromaticity.[34] To quantitatively display the contribution of delocalized β-electrons to the aromaticity, we have made a comparison with two representative clusters, Au_6 and Au_{10}^{2+}, of which both geometry and electron configuration are similar to Pt_6^- and Pt_{10}^-, respectively, but there is a lack of

https://doi.org/10.1021/acs.jpclett.1c01178
J. Phys. Chem. Lett. 2021, 12, 5115−5122

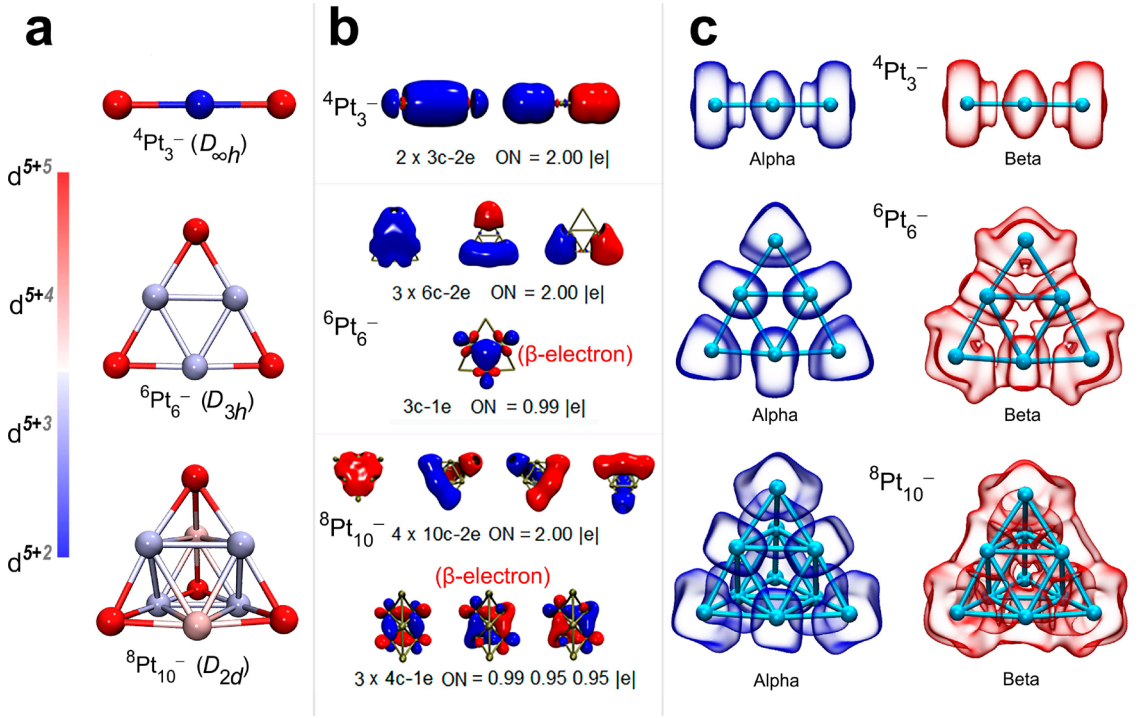

Figure 3. (a) Optimized lowest-energy structures of the $Pt_{3,6,10}^-$ clusters, where the atoms labeled in different colors show a variety of valence d electron residence. (b) AdNDP analysis showing the multicenter bondings in the $Pt_{3,6,10}^-$ clusters, where the unique beta-electron patterns are also displayed. (c) 3D-ELF analysis of the alpha and beta electrons in Pt_3^-, Pt_6^-, and Pt_{10}^- clusters, isovalue = 0.3.

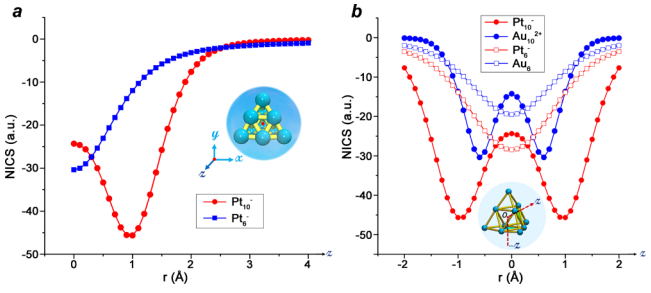

Figure 4. (a) Scan of NICS-iso of Pt_6^- (blue), and Pt_{10}^- (red) clusters from the center of them to 4 Å away along *X*-axis, with the insets showing the ground-state structures of Pt_{10}^-. (b) Comparison of the NICS-scan for the Au_6 (hollow blue dot line), Pt_6^- (hollow red dot line), Au_{10}^{2+} (blue dot line), and Pt_{10}^- (red dot line) clusters.

beta-delocalized electrons. As shown in Figure 4b, the NICS values of Pt_6^- and Pt_{10}^- are significantly larger than that of Au_6 and Au_{10}^{2+},[35] respectively, showing the distinct contribution of β-electrons to the all-metal aromaticity and dynamic stability (for details see Figures S35–36).

The pseudo-T_d Pt_{10}^- cluster contains six central Pt atom (Pt_c) and four apex Pt atoms (Pt_a) located at the four triangle-surface centers of the inner octahedral Pt_6 fragment. Also, the Pt_c–Pt_a bond distances are shorter and bond orders are larger comparing with that of Pt_c–Pt_c (Table S2), indicating stronger interactions between the Pt_4 and Pt_6 motifs than that between Pt_c and Pt_c in the octahedral Pt_6 cage. On the basis of the charge distribution, electrostatic surface potential (ESP), as well as the d electron transfer among Pt_{10}^- (Figure 3a and Figure S17), one can assign the charge as −1 for $[Pt_4]$ and 0 for the $[Pt_6]$ unit, which is similar to the four corner Ag atoms of T_d–Ag_{20} cluster. Note that, for the ground states of the Pt_3^-, Pt_6^-, and Pt_{10}^- anions, the extra electron for each is mainly located on the external apex atoms (Figure S17), being consistent with the feature that such external apex atoms correspond to the ones with the lowest coordination.

Figure 5 displays the Kohn–Sham MO energy-level correlations between $[Pt_6]$ and $[Pt_4]^-$, illustrating the origin

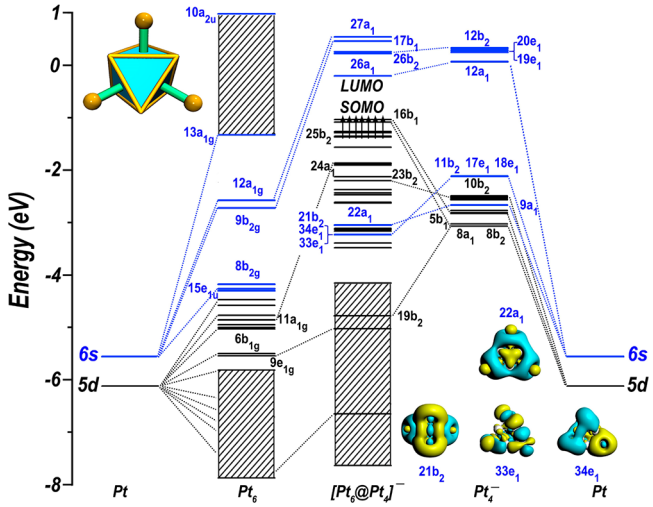

Figure 5. Kohn–Sham energy-level correlation diagram of pseudo-T_d $[Pt_6@Pt_4]^-$ cluster at the SR-ZORA PBE/TZ2P level of theory. The 6s- and 5d-based orbitals are marked in blue and black, respectively.

of stability of the pseudo-T_d-$[Pt_6@Pt_4]^-$ cluster. Inasmuch as the Pt 6s orbital has larger radial distribution than 5d orbitals, the 6s manifolds show a much larger energy range than the 5d ones. The 6s–based MOs of the T_d-$[Pt_4]^-$ transform as "$9a_1$ + $11b_2$ + $17e_1$+ $18e_1$", which contributes to the interaction with the Pt_6 moiety, corresponding to the occupied bonding MOs

https://doi.org/10.1021/acs.jpclett.1c01178
J. Phys. Chem. Lett. 2021, 12, 5115–5122

with $22a_1$, $21b_2$, $33e_1$, and $34e_1$ irreducible representations in the T_d-$[Pt_6@Pt_4]^-$ cluster (inset in Figure 5). The bonding and antibonding orbitals show a wide energy region and obvious energy gap pertaining to strong Pt_a-Pt_c and interactions. In contrast, there are weak orbital overlaps between Pt atoms in the O_h-$[Pt_6]$ unit, allowing all the 5d-based MOs contributing to the occupied orbitals while the 6s−based MOs to the unoccupied orbitals of the $[Pt_6@Pt_4]^-$. Consequently, most bonding MOs in $[Pt_6@Pt_4]^-$ are stabilized by strong interactions with the 5d-based MOs of Pt_6 moiety.

Also, all the bonding 6s-based MOs (mainly contributed by the Pt_4^- unit) are fully occupied while the antibonding 6s-based MOs are vacant, corresponding to three-dimensional all-metal aromaticity,[34,36] with $n = 1$ at a configuration of $(33e_1)^2(34e_1)^2(21b_2)^2(22a_1)^2$, which is also consistent with the PDOS analysis (Figure S18). The orbital interaction analysis is coincident with the four 10c−2e delocalized bonds given by AdNDP analysis (Figure 6). The 5d-based MOs of $[Pt_6@Pt_4]^-$

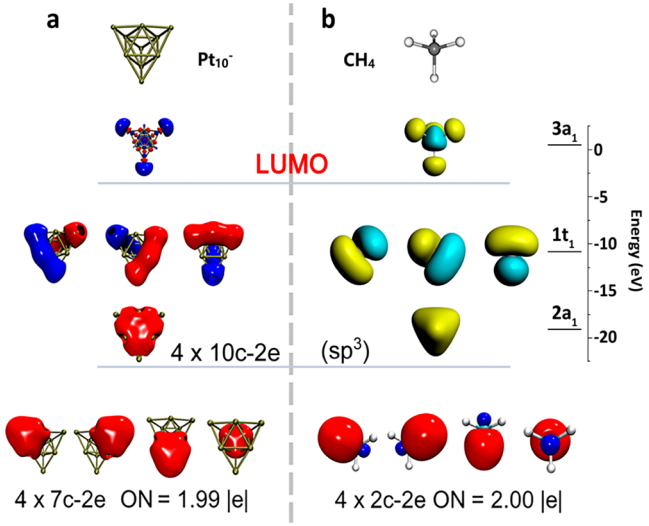

Figure 6. Comparison of the geometry, Kohn−Sham MOs and localized natural bonding orbitals of (a) Pt_{10}^- and (b) CH_4 based on AdNDP analysis.

cluster can be further divided into two regions: 43 fully occupied MOs and 7 singly occupied MOs (SOMOs). The Pt_{10}^- consists of a half-filled open-shell configuration, $(25b_2)^1(40e_1)^2(41e_1)^2(16a_2)^1(16b_1)^1$. As is shown, there is strong spin polarization in this system: for example, the alpha- and beta-MO of $26a_1$ is split as large as 0.5 eV, resulting in an alpha orbital energy gap of 0.9 eV between SOMO and LUMO. On this basis, the magic stability of Pt_{10}^- can also be understood by the modeling of a superatomic molecule.[37,38]

Figure 6 presents a comparison between the electronic layout of outer s orbitals for Pt_{10}^-, and the electron configuration of CH_4, including similar LUMO diagrams, 10c−2e multicenter bonding of Pt_{10}^- versus sp^3 hybridization of CH_4. Also, the 7c−2e multicenter bonding pattern of Pt_{10}^- closely resembles the 2c−2e of CH_4 molecule, shedding light on the σ-aromaticity,[39−41] and superatom−atom bondings.[38] These comparable bonding patterns account for the reasonable stability of the Pt_{10}^- cluster in mimicking a methane molecule. On the other hand, from the canonical molecular orbital patterns, the superatomic feature (1S|1P|2S|2P) of Pt_{10}^- are also seen for both alpha and beta orbitals (Figure S24). As a comparison, we have also calculated the frontier orbitals of BH_4^- and BF_4^- (Figure S37). As results, they both display similar sp3 hybridization, but the LUMO of BH_4^- slightly differs from LUMO of Pt_{10}^-; and the HOMO and HOMO−1 orbitals of BF_4^- differ from that of the Pt_{10}^- cluster.

Further, we provide here a comparison and discussion on the electronic transfer and bonding nature for Pt_{10}^- (M = 8), Pt_{10} (M = 9), and Pt_{10}^+ (M = 8) clusters. In addition to the interesting difference of spin multiplicity of the three clusters, their d orbitals on the outermost four Pt atoms of a tetrahedron are all filled with α and β electrons (d^{5+5}). For the cluster Pt_{10}^- within D_{2d} symmetry, the middle six atoms show different characteristics: the opposite two atoms (pink in color, Figure 3a) are occupied with five α electrons and four β electrons (d^{5+4}), while the other four atoms (gray in color) are occupied with five α electrons and three β electrons (d^{5+3}, ten electrons less). The β electrons (seven less than α electrons) of the four Pt atoms in the middle form three 4c−1e bonds suggest planar β aromaticity that also follows the Hückel $(4n + 2)$ rule. In comparison, the neutral cluster Pt_{10} of T_d symmetry allows the central six atoms to be identical with each other, and exhibits a configuration of five α electrons and three β electrons (d^{5+3}); meanwhile, β electrons of the six Pt atoms in the center form four 6c−1e bonds (i.e., the β electrons are only eight less than α electrons), shedding light on the tetrahedral β aromaticity which complies with the $2(n+1)^2$ rule. Additionally, the cluster Pt_{10}^+ also has a D_{2d} symmetry, of which the opposite two atoms in the center are occupied by five α electrons and four β electrons (d^{5+4}), but the other four atoms are occupied by four α electrons and three β electrons (d^{4+3}, β electrons are eight less) respectively. The β electrons of the Pt_{10}^+ cluster also form polycentric bonds of three 4c−1e bonds, while β electrons of the six Pt atoms in the center form four 6c−1e bonds (details in Figure S33). Moreover, for the three clusters $Pt_{10}^{\pm,0}$, their outermost s orbitals on the whole molecule form four 10c−2e bonds, shedding light on the all-metal aromaticity,[34,42,43] and in agreement with both spherical $2(n+1)^2$ and cubic $(6n+2)$ aromatic rules.

In summary, we report a joint experimental and theoretical investigation into the stability and gas-phase reactivity of pure metal clusters Pt_n^-. We observed clean and well-resolved Pt_n^- cluster distribution at $3 \le n \le 19$ and performed downstream reactions with N_2, CO_2, and CH_3Br in a compact flow tube. As results, the prominent stability of Pt_6^- and Pt_{10}^- clusters were identified by noting their inertness in the diverse reactions and the theoretically determined geometric and electronic structures of the Pt_n^- ($n = 2-14$) clusters, as well as their resulted energetics. In addition, the stability of Pt_6^- and Pt_{10}^- was found to be associated with both 6s-based regular σ-aromaticity and 5d-based unique β aromaticity originated from novel multicenter bonds, which is unveiled by AdNDP analysis and Kohn−Sham energy-level correlation diagram for the pseudo-T_d $[Pt_6@Pt_4]^-$ cluster. It is interesting that the underlined superatom−atom bonding nature of such a ten-atom metal cluster allowing to mimic the sp^3 hybridization of CH_4. This joint experimental and theoretical work adds new insights into metal cluster stability without geometric or electronic shell closure, enabling to use such superatom clusters as the structural gene for new materials.

EXPERIMENTAL AND THEORETICAL METHODS

Experimental Section. This study is based on a homemade reflection time-of-flight mass spectrometer (Re-

https://doi.org/10.1021/acs.jpclett.1c01178
J. Phys. Chem. Lett. 2021, 12, 5115−5122

TOFMS)[44] combined with the newly developed pulsed laser vaporization cluster source (LaVa)[30,45−47] and a customized compact flow tube reactor.[48−52] A pulsed 532 nm Nd:YAG laser (10 Hz) with an energy of 15−35 mJ per pulse was used to generate the pure platinum clusters with good mass resolution via a cluster formation nozzle of 35 mm length (Φ = 1.35 mm) by ablation of a platinum disk (Φ = 16 mm, 99.99% purity) in the presence of a He carrier gas (1.0 MPa, 99.999% purity) which is controlled by a pulsed general valve (Parker, Serial 9). To obtain the continuous and stable Pt clusters, the Pt disk is set for a translational and rotational motion controlled by an eccentric gear set. After the cluster was generated under the supersonic expansion, the downstream reactions between prepared pure platinum cluster anions and reactant gas were performed at room temperature. Different amount of N_2/He (20%), CO_2/He (20%) as well as CH_3Br/He (5%) at 0.1 MPa was introduced by another pulsed general valve to react with Pt_n^- clusters in the reaction tube (Φ = 6 mm and length = 60 mm). Then the product cluster anions were skimmed into a differentially pumped chamber with a high vacuum (<10^{-5} Pa), in which the molecular beam was orthogonally accelerated by positive electrodes before entering the reflector so that the instantaneous anions could be detected by a dual microchannel plate (MCP) detector. The signals from the MCP were recorded using a digital oscilloscope (Teledyne LeCroy HDO6000) by averaging 1000 traces of the independent mass spectrum.

Computational. Previous investigations have studied the geometry and properties of small Pt clusters;[38,53−56] the stability and electron configuration of the small Pt clusters have been predicted.[57,58] The low-energy structures of Pt_n^-, Pt_n, and Pt_n^+ (n = 2−15) clusters are located by unbiased global search with the combination of genetic algorithm (GA) and density functional theory (DFT) method, which have been successfully applied in the structural predictions of many systems.[59−61] A basis set LANL2DZ and a loose convergence criterion are adopted in the global search procedure, and a variety of spin multiplicities of Pt clusters are taken into account. The low-lying candidates are then fully relaxed using the PBE function[62] with D3BJ correction at the dhf-TZVP basis set.[63] All the calculations including energetics, frequencies and HOMO−LUMO gaps are based on the optimized lowest energy structures, corrected with zero-point vibration energies (ZPVE). The thresholds for the convergence of the total energy and geometry optimization were set to be 10^{-4} a.u., and all the procedures meet this criterion.

Relativistic quantum chemical studies were performed using DFT implemented in Gaussian 16 package[64] and Amsterdam Density Functional (ADF) program.[65,66] The generalized gradient approximation (GGA)[67,68] with the PBE exchange-correlation functional was used to figure out the fragments orbital interaction, together with the uncontracted TZ2P Slater basis sets for all the atoms. Frozen core approximations are applied to the inner shells [$1s^2$−$3d^{10}$] for Pt atoms and the [$4s^24p^64d^{10}5s^25p^65d^96s^1$] electrons are treated variationally. The scalar relativistic (SR) effects are considered by the zero-order regular approximation (ZORA) to account for the mass−velocity and Darwin effects.

The nucleus independent chemical ships (NICS)[69] are performed at the PBE-D3/def2-TZVP level.[70] Moreover, at dhf-TZVP basis set for Pt atoms and def2-TZVP basis set for N atoms, HOMO−LUMO gap, incremental binding energy (IBE) and the second-order binding energy (Δ_2E) of $Pt_n^{\pm,0}$ (n = 2−14) clusters, as well as their N_2-binding (E_b-N_2) energies are calculated, based on the definitions as below

$$\mathrm{IBE}(Pt_n) = E(Pt^{\pm,0}) + E(Pt_{n-1}^{\pm,0}) - E(Pt_n^{\pm,0}) \quad (5)$$

$$\Delta_2 E = E(Pt_{n+1}^{\pm,0}) + E(Pt_{n-1}^{\pm,0}) - 2E(Pt_n^{\pm,0}) \quad (6)$$

$$E_{b-N2} = E(Pt_n^{\pm,0}N_2) - E(Pt_n^{\pm,0}) - E(N_2) \quad (7)$$

Chemical bonding analysis is performed using the adaptive natural density partitioning (AdNDP)[71] by Multiwfn.[72] Molecular visualization is realized using VMD software.[73]

■ ASSOCIATED CONTENT

Supporting Information

The Supporting Information is available free of charge at https://pubs.acs.org/doi/10.1021/acs.jpclett.1c01178.

Comparable reactions of the cationic and anionic Pt clusters, theoretical results of the structures of $Pt_n^{\pm,0}$ and $Pt_nN_2^{\pm,0}$ clusters, charge distribution, density of states, molecular dynamics simulation, aromaticitic properties, superatomic orbitals, ELF and AdNDP analyses, as well as a comparison with H_3^-, Au_6, and Au_{10}^{2+} (PDF)

■ AUTHOR INFORMATION

Corresponding Authors

Longjiu Cheng − *Department of Chemistry, Anhui University, Hefei 230601, China; Key Laboratory of Structure and Functional Regulation of Hybrid Materials (Anhui University), Ministry of Education, Hefei 230601, PR China;* orcid.org/0000-0001-7086-6190; Email: clj@ustc.edu

Zhixun Luo − *State Key Laboratory for Structural Chemistry of Unstable and Stable Species, Institute of Chemistry, Chinese Academy of Sciences, Beijing 100190, China;* orcid.org/0000-0002-5752-1996; Email: zxluo@iccas.ac.cn

Authors

Yuhan Jia − *State Key Laboratory for Structural Chemistry of Unstable and Stable Species, Institute of Chemistry, Chinese Academy of Sciences, Beijing 100190, China; University of Chinese Academy of Sciences, Beijing 100049, China*

Xinlei Yu − *Department of Chemistry, Anhui University, Hefei 230601, China; Key Laboratory of Structure and Functional Regulation of Hybrid Materials (Anhui University), Ministry of Education, Hefei 230601, PR China*

Hanyu Zhang − *State Key Laboratory for Structural Chemistry of Unstable and Stable Species, Institute of Chemistry, Chinese Academy of Sciences, Beijing 100190, China;* orcid.org/0000-0002-9745-234X

Complete contact information is available at: https://pubs.acs.org/10.1021/acs.jpclett.1c01178

Author Contributions

†Y.J. and X.Y. contributed equally to this work.

Notes

The authors declare no competing financial interest.

■ ACKNOWLEDGMENTS

Financial support for this work was provided by the National Natural Science Foundation of China (Grant No. 21722308, 21873001), by Key Research Program of Frontier Sciences (CAS, Grant QYZDBSSW-SLH024), by the National Project

Development of Advanced Scientific Instruments Based on Deep Ultraviolet Laser Source (No. Y31M0112C1), and by the Beijing Natural Science Foundation (2192064).

REFERENCES

(1) Debe, M. K. Electrocatalyst approaches and challenges for automotive fuel cells. *Nature* **2012**, *486* (7401), 43−51.

(2) Belgued, M.; Pareja, P.; Amariglio, A.; Amariglio, H. Conversion of methane into higher hydrocarbons on platinum. *Nature* **1991**, *352* (6338), 789−790.

(3) Shelef, M.; McCabe, R. W. Twenty-five years after introduction of automotive catalysts: what next? *Catal. Catal. Today* **2000**, *62* (1), 35−50.

(4) Burch, R.; Breen, J. P.; Meunier, F. C. A review of the selective reduction of NO_x with hydrocarbons under lean-burn conditions with non-zeolitic oxide and platinum group metal catalysts. *Appl. Catal., B* **2002**, *39* (4), 283−303.

(5) Moses-DeBusk, M.; Yoon, M.; Allard, L. F.; Mullins, D. R.; Wu, Z.; Yang, X.; Veith, G.; Stocks, G. M.; Narula, C. K. CO oxidation on supported single Pt atoms: experimental and ab initio density functional studies of CO interaction with Pt atom on theta-Al_2O_3(010) surface. *J. Am. Chem. Soc.* **2013**, *135* (34), 12634−12645.

(6) DeRita, L.; Dai, S.; Lopez-Zepeda, K.; Pham, N.; Graham, G. W.; Pan, X.; Christopher, P. Catalyst Architecture for Stable Single Atom Dispersion Enables Site-Specific Spectroscopic and Reactivity Measurements of CO Adsorbed to Pt Atoms, Oxidized Pt Clusters, and Metallic Pt Clusters on TiO_2. *J. Am. Chem. Soc.* **2017**, *139* (40), 14150−14165.

(7) Cutillas, N.; Yellol, G. S.; de Haro, C.; Vicente, C.; Rodríguez, V.; Ruiz, J. Anticancer cyclometalated complexes of platinum group metals and gold. *Coord. Chem. Rev.* **2013**, *257* (19−20), 2784−2797.

(8) Koster, A. M.; Calaminici, P.; Orgaz, E.; Roy, D. R.; Reveles, J. U.; Khanna, S. N. On the ground state of Pd_{13}. *J. Am. Chem. Soc.* **2011**, *133* (31), 12192−12196.

(9) Imaoka, T.; Kitazawa, H.; Chun, W.-J.; Omura, S.; Albrecht, K.; Yamamoto, K. Magic Number Pt_{13} and Misshapen Pt_{12} Clusters: Which One is the Better Catalyst? *J. Am. Chem. Soc.* **2013**, *135* (35), 13089−13095.

(10) Imaoka, T.; Akanuma, Y.; Haruta, N.; Tsuchiya, S.; Ishihara, K.; Okayasu, T.; Chun, W. J.; Takahashi, M.; Yamamoto, K. Platinum clusters with precise numbers of atoms for preparative-scale catalysis. *Nat. Commun.* **2017**, *8* (1), 688.

(11) Green, A. E.; Justen, J.; Schollkopf, W.; Gentleman, A. S.; Fielicke, A.; Mackenzie, S. R. IR Signature of Size-Selective CO_2 Activation on Small Platinum Cluster Anions, Pt_n^- (n = 4−7). *Angew. Chem., Int. Ed.* **2018**, *57* (45), 14822−14826.

(12) Adlhart, C.; Uggerud, E. Reactions of platinum clusters $Pt_n^{\pm}$, n = 1−21, with CH_4: to react or not to react. *Chem. Commun.* **2006**, No. 24, 2581−2582.

(13) Roach, P. J.; Woodward, W. H.; Castleman, A. W., Jr.; Reber, A. C.; Khanna, S. N. Complementary active sites cause size-selective reactivity of aluminum cluster anions with water. *Science* **2009**, *323* (5913), 492−495.

(14) Wei, G. F.; Liu, Z. P. Subnano Pt Particles from a First-Principles Stochastic Surface Walking Global Search. *J. Chem. Theory Comput.* **2016**, *12* (9), 4698−4706.

(15) Ma, J. B.; Wang, Z. C.; Schlangen, M.; He, S. G.; Schwarz, H. On the Origin of the Surprisingly Sluggish Redox Reaction of the N_2O/CO Couple Mediated by $[Y_2O_2]^+$. and $[YAlO_2]^+$. Cluster Ions in the Gas Phase. *Angew. Chem., Int. Ed.* **2013**, *52* (4), 1226−1230.

(16) Tsunoyama, H.; Shibuta, M.; Nakaya, M.; Eguchi, T.; Nakajima, A. Synthesis and Characterization of Metal-Encapsulating Si_{16} Cage Superatoms. *Acc. Chem. Res.* **2018**, *51* (8), 1735−1745.

(17) Burgert, R.; Schnöckel, H.; Grubisic, A.; Li, X.; Stokes, S. T.; et al. Spin Conservation Accounts for Aluminum Cluster Anion Reactivity Pattern with O_2. *Science* **2008**, *319*, 438−442.

(18) Luo, Z.; Gamboa, G. U.; Smith, J. C.; Reber, A. C.; Reveles, J. U.; Khanna, S. N.; Castleman, A. W., Jr. Spin accommodation and reactivity of silver clusters with oxygen: the enhanced stability of Ag_{13}^-. *J. Am. Chem. Soc.* **2012**, *134* (46), 18973−18978.

(19) Luo, Z.; Grover, C. J.; Reber, A. C.; Khanna, S. N.; Castleman, A. W., Jr. Probing the magic numbers of aluminum-magnesium cluster anions and their reactivity toward oxygen. *J. Am. Chem. Soc.* **2013**, *135* (11), 4307−4313.

(20) Yin, B.; Du, Q.; Geng, L.; Zhang, H.; Luo, Z.; Zhou, S.; Zhao, J. Superatomic Signature and Reactivity of Silver Clusters with Oxygen: Double Magic Ag_{17}^- with Geometric and Electronic Shell Closure. *CCS Chemistry* **2021**, *3*, 219−229.

(21) Knight, W. D.; et al. Electronic Shell Structure and Abundance of Sodium Clusters. *Phys. Rev. Lett.* **1984**, *52*, 2141−2143.

(22) Yin, B.; Du, Q.; Geng, L.; Zhang, H.; Luo, Z.; Zhou, S.; Zhao, J. Anionic Copper Clusters Reacting with NO: An Open-Shell Superatom Cu_{18}. *J. Phys. Chem. Lett.* **2020**, *11* (14), 5807−5814.

(23) Luo, Z.; Castleman, A. W., Jr. Special and General Superatoms. *Acc. Chem. Res.* **2014**, *47*, 2931−2940.

(24) Reber, A. C.; Khanna, S. N. Superatoms: Electronic and Geometric Effects on Reactivity. *Acc. Chem. Res.* **2017**, *50* (2), 255−263.

(25) Jena, P.; Sun, Q. Super Atomic Clusters: Design Rules and Potential for Building Blocks of Materials. *Chem. Rev.* **2018**, *118* (11), 5755−5780.

(26) Balteanu, I.; Petru Balaj, O.; Beyer, M. K.; Bondybey, V. E. Reactions of platinum clusters $^{195}Pt_n^{\pm}$, n = 1−24, with N_2O studied with isotopically enriched platinum. *Phys. Chem. Chem. Phys.* **2004**, *6* (11), 2910−2913.

(27) Hernandez, E.; Bertin, V.; Soto, J.; Miralrio, A.; Castro, M. Catalytic Reduction of Nitrous Oxide by the Low-Symmetry Pt_8 Cluster. *J. Phys. Chem. A* **2018**, *122* (8), 2209−2220.

(28) Santini, P.; Carretta, S.; Amoretti, G.; Guidi, T.; Caciuffo, R.; Caneschi, A.; Rovai, D.; Qiu, Y.; Copley, J. R. D. Spin dynamics and tunneling of the Néel vector in the Fe_{10} magnetic wheel. *Phys. Rev. B: Condens. Matter Mater. Phys.* **2005**, *71* (18), 184405.

(29) Mandado, M.; Grana, A. M.; Perez-Juste, I. Aromaticity in spin-polarized systems: can rings be simultaneously alpha aromatic and beta antiaromatic? *J. Chem. Phys.* **2008**, *129* (16), 164114.

(30) Duncan, M. A. Invited review article: laser vaporization cluster sources. *Rev. Sci. Instrum.* **2012**, *83* (4), 041101.

(31) Li, J.; Li, X.; Zhai, H. J.; Wang, L. S. Au20: A tetrahedral cluster. *Science* **2003**, *299* (5608), 864−867.

(32) Schleyer, P. v. R.; Maerker, C.; Dransfeld, A.; Jiao, H.; van Eikema Hommes, N. J. R. Nucleus-independent chemical shifts: A simple and efficient aromaticity probe. *J. Am. Chem. Soc.* **1996**, *118*, 6317−6318.

(33) Chen, Z. F.; Wannere, C. S.; Corminboeuf, C.; Puchta, R.; Schleyer, P. v. R. Nucleus-independent chemical shifts (NICS) as an aromaticity criterion. *Chem. Rev.* **2005**, *105* (10), 3842−3888.

(34) Cui, P.; Hu, H. S.; Zhao, B.; Miller, J. T.; Cheng, P.; Li, J. A multicentre-bonded [Zn(I)]8 cluster with cubic aromaticity. *Nat. Commun.* **2015**, *6*, 6331.

(35) Petrar, P. M.; Sárosi, M. B.; King, R. B. Au102+: A Tetrahedral Cluster Exhibiting Spherical Aromaticity. *J. Phys. Chem. Lett.* **2012**, *3* (22), 3335−3337.

(36) Geng, L.; Weng, M.; Xu, C.-Q.; Zhang, H.; Cui, C.; Wu, H.; Chen, X.; Hu, M.; Lin, H.; Sun, Z.-D.; et al. $Co_{13}O_8$—Metal-loxocubes: A new class of perovskite-like neutral clusters with cubic aromaticity. *Natl. Sci. Rev.* **2021**, *8* (1), nwaa201.

(37) Cheng, L.; Yang, J. Communication: New insight into electronic shells of metal clusters: Analogues of simple molecules. *J. Chem. Phys.* **2013**, *138* (14), 141101.

(38) Cheng, L.; Zhang, X.; Jin, B.; Yang, J. Superatom-atom superbonding in metallic clusters: a new look to the mystery of an Au_{20} pyramid. *Nanoscale* **2014**, *6* (21), 12440−12444.

(39) Lin, L.; Holtzl, T.; Gruene, P.; Claes, P.; Meijer, G.; Fielicke, A.; Lievens, P.; Nguyen, M. T. Fluxionality and sigma-aromaticity in small yttrium-doped gold clusters. *ChemPhysChem* **2008**, *9* (17), 2471−2474.

https://doi.org/10.1021/acs.jpclett.1c01178
J. Phys. Chem. Lett. 2021, 12, 5115−5122

(40) Ma, F.; Li, R.-Y.; Li, Z.-R.; Chen, M.-M.; Xu, H.-L.; Li, Z.-J.; Wu, D.; Li, Z.-S. Out-of-plane sigma-aromaticity and enhanced pi-aromaticity in superatom compounds $Li_3^+N_4^{2-}M_3^+$ (M = Li, Na and K). *J. Mol. Struct.: THEOCHEM* **2009**, *913* (1−3), 80−84.
(41) Zhang, X.; Liu, G.; Gantefor, G.; Bowen, K. H.; Alexandrova, A. N. $PtZnH_5^-$, A sigma-Aromatic Cluster. *J. Phys. Chem. Lett.* **2014**, *5* (9), 1596−1601.
(42) Kuznetsov, A. E.; Birch, K. A.; Boldyrev, A. I.; Li, X.; Zhai, H. J.; Wang, L. S. All-metal antiaromatic molecule: rectangular Al_4^{4-} in the $Li_3Al_4^-$ anion. *Science* **2003**, *300*, 622−625.
(43) Li, X. L.; Kuznetsov, A. E.; Zhang, H. F.; Boldyrev, A. I.; Wang, L. S. Observation of all-metal aromatic molecules. *Science* **2001**, *291* (5505), 859−861.
(44) Zhang, H.; Wu, H.; Jia, Y.; Geng, L.; Luo, Z.; Fu, H.; Yao, J. An integrated instrument of DUV-IR photoionization mass spectrometry and spectroscopy for neutral clusters. *Rev. Sci. Instrum.* **2019**, *90* (7), 073101.
(45) Leuchtner, R. E.; Harms, A. C.; Castleman, A. W., Jr. Thermal metal cluster anion reactions: Behavior of aluminum clusters with oxygen. *J. Chem. Phys.* **1989**, *91* (4), 2753−2754.
(46) Zimmerman, J. A.; Eyler, J. R.; Bach, S. B. H.; McElvany, S. W. ″Magic number″ carbon clusters: Ionization potentials and selective reactivity. *J. Chem. Phys.* **1991**, *94* (5), 3556−3562.
(47) Wang, L. S.; Cheng, H. S.; Fan, J. Photoelectron spectroscopy of size-selected transition metal clusters: Fe_n^-, n = 3−24. *J. Chem. Phys.* **1995**, *102* (24), 9480−9493.
(48) Eller, K.; Schwarz, H. Organometallic chemistry in the gas-phase. *Chem. Rev.* **1991**, *91* (6), 1121−1177.
(49) Veldeman, N.; Lievens, P.; Andersson, M. Size-dependent carbon monoxide adsorption on neutral gold clusters. *J. Phys. Chem. A* **2005**, *109* (51), 11793−11801.
(50) Dong, F.; Heinbuch, S.; Xie, Y.; Bernstein, E. R.; Rocca, J. J.; Wang, Z. C.; Ding, X. L.; He, S. G. C═C bond cleavage on neutral $VO_3(V_2O_5)_n$ clusters. *J. Am. Chem. Soc.* **2009**, *131* (3), 1057−1066.
(51) Kerpal, C.; Harding, D. J.; Rayner, D. M.; Fielicke, A. Small Platinum Cluster Hydrides in the Gas Phase. *J. Phys. Chem. A* **2013**, *117* (34), 8230−8237.
(52) Ferrari, P.; Vanbuel, J.; Janssens, E.; Lievens, P. Tuning the Reactivity of Small Metal Clusters by Heteroatom Doping. *Acc. Chem. Res.* **2018**, *51* (12), 3174−3182.
(53) Ankudinov, A. L.; Rehr, J. J.; Low, J. J.; Bare, S. R. Sensitivity of Pt X-ray Absorption Near Edge Structure to the Morphology of Small Pt Clusters. *J. Chem. Phys.* **2002**, *116* (5), 1911−1919.
(54) Kumar, V.; Kawazoe, Y. Evolution of atomic and electronic structure of Pt clusters: Planar, layered, pyramidal, cage, cubic, and octahedral growth. *Phys. Rev. B: Condens. Matter Mater. Phys.* **2008**, *77* (20), 205418.
(55) Chaves, A. S.; Rondina, G. G.; Piotrowski, M. J.; Tereshchuk, P.; Da Silva, J. L. The role of charge states in the atomic structure of Cu_n and Pt_n (n = 2−14 atoms) clusters: a DFT investigation. *J. Phys. Chem. A* **2014**, *118* (45), 10813−10821.
(56) Fung, V.; Jiang, D.-e. Exploring structural diversity and fluxionality of Pt_n^- (*n* = 10−13) clusters from first-principles. *J. Phys. Chem. C* **2017**, *121* (20), 10796−10802.
(57) Bhattacharyya, K.; Majumder, C. Growth pattern and bonding trends in Pt (*n* = 2−13) clusters: Theoretical investigation based on first principle calculations. *Chem. Phys. Lett.* **2007**, *446* (4−6), 374−379.
(58) Ferrari, P.; Hansen, K.; Lievens, P.; Janssens, E. Stability of small cationic platinum clusters. *Phys. Chem. Chem. Phys.* **2018**, *20* (46), 29085−29090.
(59) Li, L.; Cheng, L. First principle structural determination of $(B_2O_3)_n$ (*n* = 1−6) clusters: from planar to cage. *J. Chem. Phys.* **2013**, *138* (9), 094312.
(60) Tian, Z.; Cheng, L. Perspectives on the energy landscape of Au−Cl binary systems from the structural phase diagram of Au_xCl_y (*x* + *y* = 20). *Phys. Chem. Chem. Phys.* **2015**, *17* (20), 13421−13428.
(61) Liu, Q.; Xu, C.; Cheng, L. Structural and electronic properties of bano-brass: Cu_xZn_y (*x* + *y* = 11−13) clusters. *J. Cluster Sci.* **2019**, 1−7.
(62) Grimme, S.; Antony, J.; Ehrlich, S.; Krieg, H. A consistent and accurate ab initio parametrization of density functional dispersion correction (DFT-D) for the 94 elements H-Pu. *J. Chem. Phys.* **2010**, *132* (15), 154104.
(63) Weigend, F. Accurate coulomb-fitting basis sets for H to Rn. *Phys. Chem. Chem. Phys.* **2006**, *8* (9), 1057−1065.
(64) Ogliaro, F.; Bearpark, M.; Heyd, J.; Brothers, E.; Kudin, K.; Staroverov, V.; Keith, T.; Kobayashi, R.; Normand, J.; Raghavachari, K. et al. *Gaussian 16*, revision C.01; Gaussian, Inc.: Wallingford, CT, 2016.
(65) Baerends, E. J.; Ziegler, T.; Autschbach, J.; Bashford, D.; Bérces, A.; Bickelhaupt, F.; Bo, C.; Boerrigter, P.; Cavallo, L.; Chong, D. ADF2018. *SCM*; Theoretical Chemistry, Vrije Universiteit: Amsterdam, The Netherlands.
(66) te Velde, G.; Bickelhaupt, F. M.; Baerends, E. J.; Fonseca Guerra, C.; van Gisbergen, S. J. A.; Snijders, J. G.; Ziegler, T. Chemistry with ADF. *J. Comput. Chem.* **2001**, *22* (9), 931−967.
(67) Palotas, K.; Andriotis, A. N.; Lappas, A. Structural, electronic, and magnetic properties of nanometer-sized iron-oxide atomic clusters: Comparison between GGA and GGA plus U approaches. *Phys. Rev. B: Condens. Matter Mater. Phys.* **2010**, *81* (7), 075403.
(68) Simon, L.; Goodman, J. M. How reliable are DFT transition structures? Comparison of GGA, hybrid-meta-GGA and meta-GGA functionals. *Org. Biomol. Chem.* **2011**, *9* (3), 689−700.
(69) Schleyer, P. v. R.; Maerker, C.; Dransfeld, A.; Jiao, H.; van Eikema Hommes, N. Nucleus-independent chemical shifts: a simple and efficient aromaticity probe. *J. Am. Chem. Soc.* **1996**, *118* (26), 6317−6318.
(70) Weigend, F.; Ahlrichs, R. Balanced basis sets of split valence, triple zeta valence and quadruple zeta valence quality for H to R_n: Design and assessment of accuracy. *Phys. Chem. Chem. Phys.* **2005**, *7* (18), 3297−3305.
(71) Zubarev, D. Y.; Boldyrev, A. Developing paradigms of chemical bonding: adaptive natural density partitioning. *Phys. Chem. Chem. Phys.* **2008**, *10* (34), 5207−5217.
(72) Lu, T.; Chen, F. Multiwfn: a multifunctional wavefunction analyzer. *J. Comput. Chem.* **2012**, *33* (5), 580−592.
(73) Humphrey, W.; Dalke, A.; Schulten, K. VMD: visual molecular dynamics. *J. Mol. Graphics* **1996**, *14* (1), 33−38.

https://doi.org/10.1021/acs.jpclett.1c01178
J. Phys. Chem. Lett. 2021, 12, 5115−5122